





Cite this: *Metallomics*, 2018, 10, 553

Received 25th October 2017,
Accepted 27th March 2018

DOI: 10.1039/c7mt00297a

rsc.li/metallomics

A ratiometric iron probe enables investigation of iron distribution within tumour spheroids†

Isaac J. Carney, Jacek L. Kolanowski,  Zelong Lim, Benjamin Chekroun, 
Angela G. Torrisi, Trevor W. Hambley and Elizabeth J. New *

Iron dysregulation is implicated in numerous diseases, and iron homeostasis is profoundly influenced by the labile iron pool (LIP). Tools to easily observe changes in the LIP are limited, with calcein AM-based assays most widely used. We describe here FICFe1, a ratiometric analogue of calcein AM, which also provides the capacity for imaging iron in 3D cell models.

Iron is found in a huge variety of protein active sites, having arrived in these roles due to its natural abundance and bio-availability, as well as its accessible redox chemistry.¹ In addition to its major role in the transport of oxygen by haemoglobin in erythrocytes, iron is essential to the activity of catalase, which decomposes peroxides;² acotinase, a key enzyme in the Krebs cycle;³ and cytochrome *c*, which forms part of the electron transport chain.⁴

While most iron in the body is tightly bound to proteins, either for function or for storage, a small percentage of cytosolic iron exists as an accessible reservoir known as the labile iron pool (LIP). This pool is buffered by a range of monodentate ligands at low micromolar concentrations.⁵ The reducing environment of the cell maintains the LIP primarily in the form of Fe(II), which can participate in Fenton reactions to generate damaging reactive oxygen species (ROS). As a result, the LIP is tightly-regulated by a range of iron-sensing, iron-storing and iron-chaperoning proteins centred around the IRP2/FBXL-5 axis.⁶

Quantification of the LIP is of interest across a vast range of biological and medical studies, from the interaction of immune cells with iron-scavenging bacteria,⁷ to understanding diseases of iron dysregulation such as Friedreich's ataxia,⁸ and neuro-degenerative diseases such as Alzheimer's in which iron imbalances have been implicated.⁹ The interactions of iron with cancer are also of much current interest, including observation of an

Significance to metallomics

Iron plays a key role in numerous biological systems, but studies of the labile iron pool almost exclusively use calcein AM, which gives a turn-off response in the presence of iron that can be difficult to interpret. We present here an improved analogue of calcein AM, which gives a ratiometric, turn-on and therefore more reliable response to iron. We showcase its use in imaging tumour spheroids, but this probe is suitable for broad use in elucidating the roles of iron in biology.

altered LIP in cancer,¹⁰ and iron chelation as a proposed cancer treatment.¹¹

There are a number of techniques available to measure total cellular iron levels, including histological stains, and mass spectrometric and synchrotron X-ray fluorescence techniques, which have been reviewed extensively elsewhere.¹² However, these are measures of bulk iron, and therefore cannot be used to specifically assess the LIP. Furthermore, these techniques generally involve disruption of the cellular structure and/or environment, limiting their application in the study of living cells. In contrast, microscopy with small molecule fluorescent sensors enables the selective imaging of the labile metal pool in living cells.¹³ The first-reported fluorescent sensor of the LIP, calcein AM,¹⁴ relies on a sufficient excess of iron over all other transition metals as iminodiacetate metal chelating sites do not exhibit appreciable iron selectivity. A further disadvantage of calcein AM is that it is a turn-off probe: iron binding causes quenching of fluorescence. Common protocols for its use therefore require the subsequent addition of an iron chelator to restore the fluorescence of the probe. The past two decades have seen the development of elegant alternate strategies for iron sensing,¹⁵ including turn-on sensors for Fe(III),¹⁶ the use of siderophores as the iron receptor,¹⁷ and reaction-based sensors.^{18–20} Responsive probes have also been reported that measure sub-cellular iron pools, including those in the mitochondria^{21,22} and endoplasmic reticulum.²³ However, while there has been much synthetic activity in this area, there has been limited application of new probes, with the majority of biological

School of Chemistry, The University of Sydney, NSW 2006, Australia.
E-mail: elizabeth.new@sydney.edu.au

† Electronic supplementary information (ESI) available. See DOI: 10.1039/c7mt00297a



studies of iron homeostasis continuing to use calcein AM, or even histochemical staining.

We sought to investigate whether calcein AM could be repurposed to provide auxiliary unambiguous fluorescence output, thus enhancing the information that can be derived from fluorescence studies. We addressed the primary drawback of the probe: its turn-off response to the addition of iron. The application of intensity-based probes, for which the presence of analyte is signalled by a change in emission intensity at a single wavelength, is limited by the fact that emission intensity is a factor of probe concentration and analyte concentration. Amongst intensity-based probes, analysis of data from turn-off probes is particularly difficult, as the absence of the probe is indistinguishable from the presence of the analyte. More useful data can be obtained from ratiometric probes, for which the analyte induces a change in the spectral form and the ratio of two independent peaks reports on analyte concentration, but not probe accumulation.²⁴ We report here our synthesis and characterisation of a ratiometric analogue of calcein AM, **FICFe1**, and our subsequent use of the probe to investigate iron distribution in tumour spheroids.

Our probe design involved tethering a second fluorophore to calcein AM, a strategy we have previously demonstrated to be successful in the conversion of a turn-off sensor to a ratiometric sensor.²⁵ To minimise fluorescence overlap with the green emission of calcein, we selected the blue-emitting 7-diethylaminocoumarin as the second fluorophore, to give a fluorescein coumarin iron probe, **FICFe1** (Fig. 1a). The coumarin with a *trans*-cyclohexane-1,4-diamine linker was synthesised as previously described.²⁶ 5(6)-Carboxyfluorescein was diacetate protected, and the 5(6)-carboxy group activated as an *N*-succinimidyl ester, and at this point it was possible to separate the two isomers by column chromatography.²⁷ The 5-isomer was subsequently coupled to the coumarin group, deprotected and decorated with iminodiacetic acid groups that were then acetoxymethyl ester-protected in an analogous manner to that reported for the synthesis of calcein AM,^{28,29} to give **FICFe1**.

Since acetoxymethyl ester protection leads to quenching of the fluorescence of the fluorescein group,²⁹ spectroscopic studies were performed on the non-protected precursor, **FICFe1'** (Fig. 1b). The precursor exhibited two emission peaks at 490 nm and 530 nm upon a single excitation at 405 nm (Fig. 2a), corresponding to the coumarin and fluorescein emission respectively. Addition of iron (as $(\text{NH}_4)_2\text{Fe}(\text{SO}_4)_2$) led to a decrease in the longer wavelength peak (Fig. 2a). The ratio of the emission intensities of the two peaks (blue:yellow) increased with iron addition (Fig. 2b), with

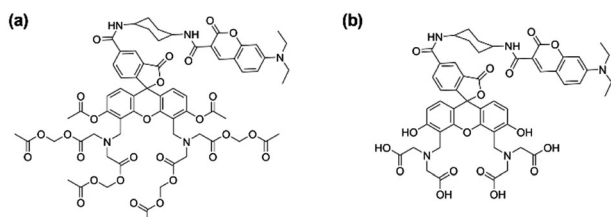


Fig. 1 (a) Structure of **FICFe1**. (b) Structure of **FICFe1'**.

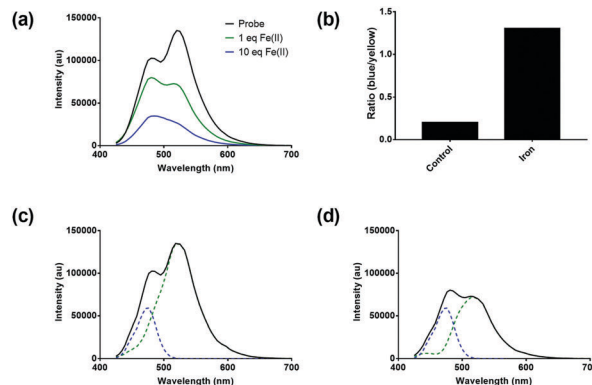


Fig. 2 (a) Emission spectra of **FICFe1'** with 1 and 10 equivalents of Fe(II) ($\lambda_{\text{ex}} = 405 \text{ nm}$). (b) Ratios of 490 nm to 530 nm emission in the absence and presence of Fe(II) ($\lambda_{\text{ex}} = 405 \text{ nm}$). (c) Deconvolution of the **FICFe1'** emission spectrum without Fe(II) . (d) Deconvolution of the **FICFe1'** emission spectrum with 1 equivalent of Fe(II) .

the deconvolution of the two peaks confirming that the coumarin peak remained unaffected by the addition of iron (Fig. 2c and d). Metal selectivity studies revealed similar selectivity to that observed for calcein (Fig. S1, ESI[†]), with similar responses to other divalent metal ions Co(II) , Ni(II) and Cu(II) , which are present at far lower concentrations in the cell than iron.^{30,31}

Having demonstrated a ratiometric response to iron in the cuvette, we investigated the emission from DLD-1 colorectal adenocarcinoma cells treated with **FICFe1**. An incubation time of 2 h was chosen, which far exceeds the reported time for the maximal hydrolysis of calcein AM (of 30 min).³² We were able to observe emission in the cytoplasm in both blue (425–480 nm) and yellow (520–600 nm) channels (Fig. S2, ESI[†]), with no specific organellar localisation. The blue-to-yellow ratio decreased in cells pre-treated with iron chelator salicylaldehyde isonicotinoyl hydrazone (SIH) (Fig. 3b), due to a decrease in yellow fluorescence, while pre-treatment with ferrous ammonium sulfate (FAS) led to lower yellow emission and therefore a higher blue-to-yellow ratio (Fig. 3c). The quantification of the blue-to-yellow ratio reveals a statistically significant increase in iron-supplemented cells, and a decrease in iron-starved cells (Fig. 3d).

Having demonstrated that **FICFe1** can report on changes in iron levels within cultured cells, we were interested in its capacity to investigate iron levels in multicellular systems. Tumour spheroids, which are 3D aggregates of cells, are an attractive *in vitro* model that provides a bridge between 2D cell cultures and tissue.³³ They are particularly useful in assessing the efficacy of anticancer drugs, especially those intended to exert an effect on cells in a solid tumour.³⁴ Despite its ubiquitous use, calcein AM is unsuitable for reporting on the labile iron pool throughout a tumour, as it stains only the outer cell layers (Fig. S3, ESI[†]). While this could be indicative of a very high iron concentration within the spheroid, which therefore quenches probe fluorescence, it is more likely to be consistent with the rapid cellular uptake of the probe, preventing its movement further into the centre of the spheroid. In contrast, **FICFe1** shows penetration into the tumour spheroid, with a measurable ratio up to 200 μm into the 3D tumour model (Fig. 4). Since the blue:yellow ratio is

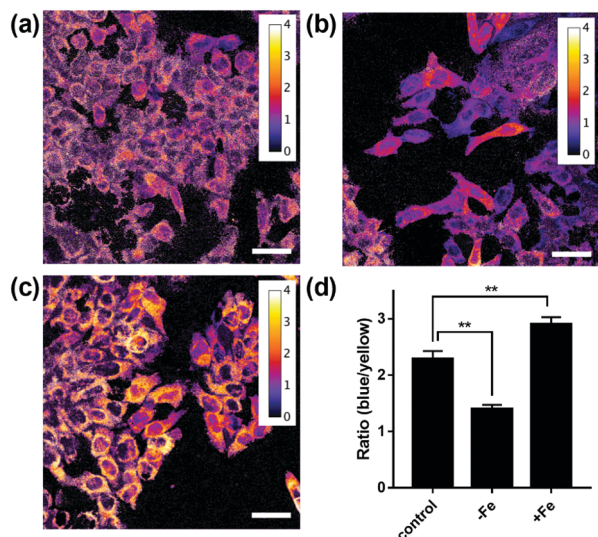


Fig. 3 FICFe1 can report on exogenous changes in iron levels. Confocal ratio images (425–480 nm/520–600 nm, $\lambda_{\text{ex}} = 405$ nm) of DLD-1 cells treated with FICFe1 (10 μM, 2 h) followed by 30 min treatment with (a) vehicle control, (b) salicylaldehyde isonicotinoyl hydrazone (SIH; 10 μM) or (c) ferrous ammonium sulfate (FAS; 100 μM). Scale bars represent 20 μm. (d) Changes in the blue/yellow ratio under different conditions. Error bars represent standard deviations of 5 replicates, ** $p < 0.01$.

not dependent on probe concentration, the ratio image reports directly on the concentration of the LIP (Fig. 4c). Furthermore, it has previously been shown that esterase activity is maintained throughout tumour spheroids,³⁵ confirming that any changes observed here are due to changes in iron levels rather than differences in the hydrolysis of acetoxymethyl esters.

Since FICFe1 can be used to study the LIP within a tumour spheroid, we sought to investigate the effects of common iron chelation agents on spheroid iron levels. There is much interest in the potential for iron chelation therapy for the treatment of

cancer,³⁶ based on the rationale that starving cancer cells of essential iron will prevent their growth. Iron chelators deferasirox and deferiprone are clinically-approved for treatment of iron overload disorders,³⁷ and have shown efficacy in cancer treatment.^{38,39} When spheroids were treated with these two chelators, a decreased FICFe1 ratio was observed at the periphery of the spheroid (the outer 20 μm), but beyond that point, iron levels were very similar to control spheroids (Fig. 4 and Fig. S4, S5, ESI†). This indicates that these iron chelators have poor tumour penetration, and therefore are likely to have little efficacy beyond the outer layers of a tumour. It will therefore be valuable in the future to study alternative iron chelators to investigate whether greater tumour penetration gives rise to better efficacy against tumours. In contrast, analogous images of spheroids treated with calcein AM and iron chelators only show measurable fluorescence in the outer one or two cell layers, and no difference between the iron treatments can be observed (Fig. S6, ESI†).

Conclusions

We have demonstrated that by adding a control fluorophore to the commonly-used turn-off calcein AM, we can generate a ratiometric and therefore significantly more reliable probe FICFe1, which operates in the same manner as its widely-used parent, providing direct information about the LIP. FICFe1 offers the added capacity for imaging 3D cell models, and can be used to study the effect of iron chelation agents on iron distribution in multicellular models. In the future, studies of this type will be further advanced by the development of probes targeted to specific sub-cellular organelles. We are now applying this system to the investigation of more complex multicellular systems and organisms.

Conflicts of interest

There are no conflicts to declare.

Acknowledgements

We acknowledge the Australian Research Council (DP150100649) for funding. E.J.N. acknowledges the Westpac Bicentennial Foundation for a Research Fellowship. We acknowledge the facilities and the scientific and technical assistance of the Australian Microscopy & Microanalysis Research Facility at the Australian Centre for Microscopy & Microanalysis at the University of Sydney.

Notes and references

- 1 P. A. Frey and G. H. Reed, *ACS Chem. Biol.*, 2012, **7**, 1477–1481.
- 2 S. J. Dixon and B. R. Stockwell, *Nat. Chem. Biol.*, 2014, **10**, 9–17.
- 3 P. J. Artymiuk and J. Green, *Structure*, 2006, **14**, 2–4.
- 4 C. Lange and C. Hunte, *Proc. Natl. Acad. Sci. U. S. A.*, 2002, **99**, 2800–2805.
- 5 R. C. Hider and X. Kong, *Dalton Trans.*, 2013, **42**, 3220–3229.

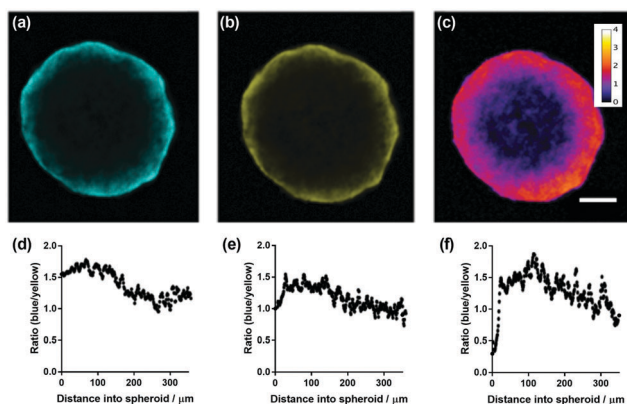


Fig. 4 Iron chelation agents only alter iron levels at the edge of the spheroid. Confocal microscopy images: (a) blue channel (425–480 nm), (b) yellow channel (520–600 nm) and (c) blue/yellow ratio images of DLD-1 spheroids (10⁶ cells) incubated with FICFe1 (10 μM, 24 h). Ratio intensity plots of spheroids subsequently treated for 2 h with (d) vehicle control, (e) deferiprone (100 μM) and (f) deferasirox (100 μM). The scale bar represents 200 μm.



- 6 T. Moroishi, M. Nishiyama, Y. Takeda, K. Iwai and K. I. Nakayama, *Cell Metab.*, 2011, **14**, 339–351.
- 7 J. E. Cassat and E. P. Skaar, *Cell Host Microbe*, 2013, **13**, 509–519.
- 8 B. Sturm, U. Bistrich, M. Schranzhofer, J. P. Sarsero, U. Rauen, B. Scheiber-Mojdehkar, H. de Groot, P. Ioannou and F. Petrat, *J. Biol. Chem.*, 2005, **280**, 6701–6708.
- 9 D. Hare, S. Ayton, A. Bush and P. Lei, *Front. Aging Neurosci.*, 2013, **5**, 34.
- 10 S. V. Torti and F. M. Torti, *Nat. Rev. Cancer*, 2013, **13**, 342–355.
- 11 L. B. Joan, M. T. Frank and V. T. Suzy, *Curr. Med. Chem.*, 2003, **10**, 1021–1034.
- 12 D. J. Hare, E. J. New, M. D. de Jonge and G. McColl, *Chem. Soc. Rev.*, 2015, **44**, 5941–5958.
- 13 E. J. New, *Dalton Trans.*, 2013, **42**, 3210–3219.
- 14 W. Breuer, S. Epsztejn, P. Millgram and I. Z. Cabantchik, *Am. J. Physiol.: Cell Physiol.*, 1995, **268**, C1354–C1361.
- 15 T. Hirayama and H. Nagasawa, *J. Clin. Biochem. Nutr.*, 2017, **60**, 39–48.
- 16 A. Goel, S. Umar, P. Nag, A. Sharma, L. Kumar, Shamsuzzama, Z. Hossain, J. R. Gayen and A. Nazir, *Chem. Commun.*, 2015, **51**, 5001–5004.
- 17 S. Noël, L. Guillon, I. J. Schalk and G. L. A. Mislin, *Org. Lett.*, 2011, **13**, 844–847.
- 18 A. T. Aron, M. O. Loehr, J. Bogen and C. J. Chang, *J. Am. Chem. Soc.*, 2016, **138**, 14338–14346.
- 19 H. Y. Au-Yeung, J. Chan, T. Chantarojsiri and C. J. Chang, *J. Am. Chem. Soc.*, 2013, **135**, 15165–15173.
- 20 T. Hirayama, K. Okuda and H. Nagasawa, *Chem. Sci.*, 2013, **4**, 1250–1256.
- 21 V. Abbate, O. Reelfs, R. C. Hider and C. Pourzand, *Biochem. J.*, 2015, **469**, 357–366.
- 22 V. Abbate, O. Reelfs, X. Kong, C. Pourzand and R. C. Hider, *Chem. Commun.*, 2016, **52**, 784–787.
- 23 M. H. Lee, H. Lee, M. J. Chang, H. S. Kim, C. Kang and J. S. Kim, *Dyes Pigm.*, 2016, **130**, 245–250.
- 24 E. J. New, *ACS Sensors*, 2016, **1**, 328–333.
- 25 C. Shen, J. L. Kolanowski, C. M. N. Tran, A. Kaur, M. C. Akerfeldt, M. S. Rahme, T. W. Hambley and E. J. New, *Metallomics*, 2016, **8**, 915–919.
- 26 A. Kaur, M. A. Haghighatbin, C. F. Hogan and E. J. New, *Chem. Commun.*, 2015, **51**, 10510–10513.
- 27 A. Brunet, T. Aslam and M. Bradley, *Bioorg. Med. Chem. Lett.*, 2014, **24**, 3186–3188.
- 28 H. Diehl and J. L. Ellingboe, *Anal. Chem.*, 1956, **28**, 882–884.
- 29 S. Izumi, Y. Urano, K. Hanaoka, T. Terai and T. Nagano, *J. Am. Chem. Soc.*, 2009, **131**, 10189–10200.
- 30 V. N. Gladyshev and Y. Zhang, *Met. Ions Life Sci.*, 2013, **12**, 529–580.
- 31 T. D. Rae, P. J. Schmidt, R. A. Pufahl, V. C. Culotta and T. V. O'Halloran, *Science*, 1999, **284**, 805–808.
- 32 D. Bratosin, L. Mitrofan, C. Palii, J. Estaquier and J. Montreuil, *Cytometry, Part A*, 2005, **66**, 78–84.
- 33 F. Pampaloni, E. G. Reynaud and E. H. K. Stelzer, *Nat. Rev. Mol. Cell Biol.*, 2007, **8**, 839–845.
- 34 K. M. Charoen, B. Fallica, Y. L. Colson, M. H. Zaman and M. W. Grinstaff, *Biomaterials*, 2014, **35**, 2264–2271.
- 35 C. E. Bigelow, S. Mitra, R. Knuechel and T. H. Foster, *Br. J. Cancer*, 2001, **85**, 727–734.
- 36 Y. Yu, E. Gutierrez, Z. Kovacevic, F. Saletta, P. Obeidy, Y. Suryo Rahmanto and D. R. Richardson, *Curr. Med. Chem.*, 2012, **19**, 2689–2702.
- 37 E. Poggiali, E. Cassinerio, L. Zanaboni and M. D. Cappellini, *Blood Transfusion*, 2012, **10**, 411–422.
- 38 M. R. Bedford, S. J. Ford, R. D. Horniblow, T. H. Iqbal and C. Tselepis, *J. Clin. Pharmacol.*, 2013, **53**, 885–891.
- 39 H. C. Hatcher, R. N. Singh, F. M. Torti and S. V. Torti, *Future Med. Chem.*, 2009, **1**, 1643–1670.

